International Journal of Solids and Structures 126–127 (2017) 1–7

Contents lists available at ScienceDirect

International Journal of Solids and Structures

journal homepage: www.elsevier.com/locate/ijsolstr

Elastic wave propagation in simple-sheared hyperelastic materials with different constitutive models

Linli Chen, Zheng Chang*, Taiyan Qin

College of Science, China Agricultural University, Beijing 100083, China

ARTICLE INFO

Article history:
Received 21 March 2017
Revised 17 July 2017
Available online 27 July 2017

Keyword:
Elastic wave
Hyperelastic
Stain energy function
Compressible

ABSTRACT

We investigate the elastic wave propagation in various hyperelastic materials which are subjected to simple-shear deformation. Two compressible types of three conventional hyperelastic models are considered. We found pure elastic wave modes that can be obtained in compressible neo-Hookean materials constructed by adding a bulk strain energy term to the incompressible strain energy function. Meanwhile, for the compressible hyperelastic models which are reformulated into deviatoric and hydrostatic parts, only quasi modes can propagate, with abnormal ray directions that can be observed for longitudinal waves. Moreover, the influences of material constants, material compressibility and external deformations on the elastic wave propagation and refraction in these hyperelastic models are systematically studied. Numerical simulations are carried out to validate the theoretical results. This investigation may open a promising route for the realization of next generation metamaterials and novel wave manipulation devices.

1. Introduction

Soft materials such as elastomers, gels and many biological tissues usually exhibit rich and complex static and dynamic behaviors when subjected to finite deformation. To describe the nonlinear mechanical behavior of such materials, hyperelasticity is usually employed. Many hyperelastic models (or Strain Energy Functions, SEFs) (Simo and Pister, 1984; Arruda and Boyce, 1993; Gent, 1996; Hartmann and Neff, 2003) are proposed based on experimental data fitting (Ogden, 1972; Yeoh, 1993; Boyce and Arruda, 2012), and hereafter applied for theoretical and numerical analyses. Recently, soft materials with hyperelastic SEFs have drawn considerable attention in the field of elastodynamics. In particular, by virtue of the high sensitivity to deformations and the remarkable capability of reversible structural instability of soft materials, soft metamaterials or soft phononic crystals (Bertoldi and Boyce, 2008; Auriault and Boutin, 2012; Wang and Bertoldi, 2012; Shim et al., 2015) with tunable or adaptive properties have been demonstrated for wave applications. Moreover, a Hyperelastic Transformation theory (Norris and Parnell, 2012; Parnell, 2012; Chang et al., 2015; Liu et al., 2016) has been reported, providing homogeneous soft materials with certain SEFs that can be utilized to manipulate elastic wave paths. In all these works, it is generally revealed that subtle differences in hyperelastic models may cause significant, or even subversive, distinctions in the performance of the soft devices. Therefore, a comprehensive understanding of the mechanical behaviors for different SEFs is essential, especially for applications where high-precision is demanded.

Hyperelastic materials are usually considered to be incompressible. However, compressible hyperelastic models are indispensable in considering the longitudinal wave motion in elastodynamic problems. There are a couple of approaches to extend an incompressible hyperelastic model to a compressible form (Boyce and Arruda, 2012). It has been demonstrated (Ehlers and Eipper, 1998) that these two versions of the SEFs have substantially different static behaviors, especially when the volume of the material changes significantly. Nevertheless, the way in which these SEFs relate to their dynamic properties is still elusive.

Moreover, a previous study (Chang et al., 2015) has proposed a feasible method to separate longitudinal and shear waves with a simple-sheared neo-Hookean solid. Considering the diversity of hyperelastic models, there remains an unmet need for understanding the capability of wave-mode separation for different hyperelastic models.

To address the aforementioned issues, in this paper, we focus on the propagation and refraction of elastic waves in simple-sheared hyperelastic materials. In the framework of Small-on-Large theory (Ogden, 2007), the dynamic behaviors of two different compressible types of the three conventional incompressible hyperelastic models are considered. We show that pure elastic wave modes may propagate in a compressible neo-Hookean model which is

* Corresponding author.
E-mail address: changzh@cau.edu.cn (Z. Chang).

http://dx.doi.org/10.1016/j.ijsolstr.2017.07.027
0020-7683/

constructed by adding a bulk strain energy term to an incompressible SEF. For a compressible model reformulated from a conventional incompressible SEF into a deviatoric part and a hydrostatic part, only quasi wave modes exist. When considering the refraction of elastic waves which are normally incident on a plane interface from an un-deformed hyperelastic material to a pre-deformed one, significant differences can be observed in the refraction angle of the longitudinal wave between the two versions of SEFs. Both theoretical analysis and numerical simulations are carried out to confirm each other. The paper is organized as follows: in Section 2, the approaches to extend the incompressible SEFs to the compressible ones are briefly reviewed; the Small-on-Large theory, which describes linear wave motion propagation in a finitely deformed hyperelastic material, is reviewed in Section 3. Moreover, the behavior of elastic wave propagation and refraction in a simple-sheared hyperelastic material with different SEFs is shown in Section 4, with numerical validations illustrated in Section 5. Finally, a discussion on our results and on the avenues for future work is provided in Section 6.

2. Strain energy functions for compressible hyperelastic materials

In this section, we briefly review the two approaches (Boyce and Arruda, 2012) for expanding an incompressible SEF into a compressible one.

Approach I involves adding a bulk strain energy term W_B to an existing incompressible isotropic SEF W_C. Thus, the compressible SEF can be expressed as

$$W_1 = W_C(I_1, I_2, J) + W_B(J), \tag{1}$$

where I_1 and I_2 are the first and second invariant of the right Cauchy–Green tensor, respectively. $J = \det(\mathbf{F})$ is the volumetric ratio. $F_{ij} = \partial x_i/\partial X_j$ denotes the deformation gradient, in which X_j and x_i are the coordinates in the initial and the current configurations, respectively.

Approach II involves applying a multiplicative decomposition on the Cauchy–Green deformation tensor, and reformulating the incompressible SEF into a deviatoric one. A hydrostatic strain energy term W_H is then added to extend the SEF into a compressible form, namely

$$W_2 = W_D\left(\bar{I}_1, \bar{I}_2\right) + W_H(J), \tag{2}$$

where $\bar{I}_1 = J^{-1}I_1$ and $\bar{I}_2 = J^{-2}I_2$ are the invariants of the deviatoric stretch tensor.

In Eqs. (1) and (2), the bulk stain energy terms W_B or W_H can be selected from some empirical formulas, such as $W_{H1}(J) = B(\ln J)^2/2$, $W_{H2}(J) = B((J^2-1)/2 - \ln J)/2$, $W_{H3}(J) = B(J-1)^2/2$, and $W_{H4}(J) = B\{\cosh[\alpha(J-1)] - 1\}/\alpha^2$, which are provided in former literature (Bischoff et al., 2001; Hartmann and Neff, 2003). In these formulas, B and α are material parameters, which can be determined from the conditions (Simo and Pister, 1984) of $W(\mathbf{F} = \mathbf{I}) = 0$, $\partial W(\mathbf{F} = \mathbf{I})/\partial \mathbf{F} = 0$ and $\partial^2 W(\mathbf{F} = \mathbf{I})/\partial \mathbf{F}\partial \mathbf{F} = \lambda\delta_{ij}\delta_{kl} + \mu\delta_{ik}\delta_{jl} + \mu\delta_{il}\delta_{jk}$.

Furthermore, specific examples are presented for future reference. All the SEFs proposed can be found in previous publications. For the sake of simplicity, we consider all the SEFs to be in their two-dimensional (2-D) forms.

A compressible model of a neo-Hookean SEF constructed by Approach I can be written as (Ogden, 1997)

$$W_{NH1} = \frac{\mu}{2}(I_1 - 2) - \mu \ln(J) + \frac{\lambda}{2}(J-1)^2, \tag{3}$$

where λ and μ are the first and the second *Lamé* constants. The corresponding form constructed by Approach II can be found as (Ehlers and Eipper, 1998)

$$W_{NH2} = \frac{\mu}{2}\left(\bar{I}_1 - 2\right) + \frac{\kappa}{2}(\ln J)^2, \tag{4}$$

where $\kappa = \lambda + \mu$ is the 2-D bulk modulus.

Similarly, two typical compressible forms of the Arruda–Boyce model can also be found in previous contributions (Boyce and Arruda, 2012; Kaliske and Rothert, 1997), which can be written as

$$\begin{aligned} W_{AB1} = C_1\Bigg[&\frac{1}{2}(I_1 - 2) + \frac{1}{20N}(I_1^2 - 4) + \frac{11}{1050N^2}(I_1^3 - 8) \\ &+ \frac{19}{7000N^3}(I_1^4 - 16) + \frac{519}{673750N^4}(I_1^5 - 32)\Bigg] \\ &- \mu \ln(J) + \frac{\lambda}{2}(J-1)^2, \end{aligned} \tag{5}$$

and

$$\begin{aligned} W_{AB2} = C_1\Bigg[&\frac{1}{2}(\bar{I}_1 - 2) + \frac{1}{20N}(\bar{I}_1^2 - 4) + \frac{11}{1050N^2}(\bar{I}_1^3 - 8) \\ &+ \frac{19}{7000N^3}(\bar{I}_1^4 - 16) + \frac{519}{673750N^4}(\bar{I}_1^5 - 32)\Bigg] \\ &+ \frac{\lambda + \mu}{2}\left(\frac{J^2 - 1}{2} - \ln J\right), \end{aligned} \tag{6}$$

where $C_1 = \mu/(1 + 2/5N + 44/175N^2 + 152/875N^3 + 834/67375N^4)$ and N is a material constant that denotes a measure of the limiting network stretch. Note that the form of C_1 used here is only for 2-D SEFs. When $N \to \infty$, the Arruda–Boyce model degenerates to the neo-Hookean model.

Another commonly utilized hyperelastic model is the Gent model (Gent, 1996). Here we only consider its compressible form as constructed by Approach I, which can be referred from an earlier work (Bertoldi and Boyce, 2008), namely

$$W_{G1} = -\frac{\mu J_m}{2}\ln\left(1 - \frac{I_1 - 2}{J_m}\right) - \mu \ln J + \left(\frac{\lambda}{2} - \frac{\mu}{J_m}\right)(J-1)^2, \tag{7}$$

where J_m is a material constant that is related to the strain saturation of the material. Similar to the Arruda–Boyce model, the Gent model also degenerates to the neo-Hookean model when $J_m \to \infty$.

3. Small-on-Large wave motion in hyperelastic materials

The Small-on-Large theory provides an ideal platform for investigating linear wave propagation in finite-deformed hyperelastic materials. For a hyperelastic solid with a certain SEF, the equilibrium equation of the finite deformation can be written as (Ogden, 2007)

$$(A_{ijkl}U_{l,k})_{,i} = 0\,, \tag{8}$$

where U_i denotes the displacement, $A_{ijkl} = \partial^2 W/\partial F_{ji}\partial F_{lk}$ are the components of the fourth-order elastic tensor expressed in the initial configuration. Furthermore, the governing equation of the linear wave motion u_i that is superimposed on the finite deformation U_i can be written as (Ogden, 2007)

$$(A_{0i'jk'l}u_{l,k})_{,i} = \rho_0 \ddot{u}_j, \tag{9}$$

where $A_{0i'jk'l} = J^{-1}F_{i'i}F_{k'k}A_{ijkl}$ and $\rho_0 = J^{-1}\rho$ are the elastic tensor and mass density of the current configurations, respectively. ρ is the density of the initial material.

For a homogenously deformed hyperelastic material, incremental plane waves can be expressed in the form of (Ogden, 2007)

$$u_i = m_i f\left(k l_j \cdot x_j - \omega t\right), \tag{10}$$

where m is a unit polarization vector, f denotes a twice continuously differentiable function, $\mathbf{l}$ is the unit vector in the wave direction, ω is the angular frequency of the elastic waves and k is the wave number. By inserting Eq. (10) into (9), the Christoffel equation can be obtained as

$$A_{0i'jk'l}l_{i'}l_{k'}m_l = c^2\rho_0 m_j\,, \tag{11}$$

where $c=\omega/k$ is the velocity of the wave. By solving the eigenvalue problem of Eq. (11), we can obtain the phase velocities (V_P and V_S) and polarization angles (ψ_P and ψ_S) of the P- and S-waves which propagate in pre-deformed hyperelastic material. The phase-slowness of the P- and S-waves can thus be yielded as $S_{P,S}=1/V_{P,S}$. Moreover, at a fixed frequency, the slowness curves that give $S_{P,S}$ as a function of the wave direction $\mathbf{l}$ can be plotted. Furthermore, the ray velocities of the P- and S-waves can be obtained by the rule of $\mathbf{V}^r_{P,S}\cdot\mathbf{l}=V_{P,S}$ (Auld, 1973). The slopes of the ray directions can be expressed as functions of the wave direction as shown in (Chang et al., 2015)

$$\tan\varphi_{P,S}=\frac{S_{P,S}\sin\varphi-(\mathrm{d}S_{P,S}/\mathrm{d}\varphi)\cos\varphi}{S_{P,S}\cos\varphi+(\mathrm{d}S_{P,S}/\mathrm{d}\varphi)\sin\varphi}, \tag{12}$$

where $\varphi=\arctan(l_y/l_x)$ is the wave direction, $\varphi_P=\arctan(V^r_{Py}/V^r_{Px})$ and $\varphi_S=\arctan(V^r_{Sy}/V^r_{Sx})$ denote the directions of the rays.

To consider the refraction of elastic waves on a plane interface between two homogeneously pre-deformed hyperelastic materials, the refraction angles of the elastic waves can be obtained by the graphical method proposed by a previous study (Rokhlin et al., 1985). In this work, we particularly consider the refraction of elastic waves normally incident on a plane interface from an undeformed hyperelastic material to a pre-deformed one. In this case, the refraction angles are $\theta_{P,S}=\phi_{P,S}$ for any given ϕ. We define the separation angle as $\Delta\theta=|\theta_S-\theta_P|$ in order to examine the difference between the P- and S-waves.

4. Elastic wave propagation in simple-sheared hyperelastic materials

We first consider the propagation of P- and S-waves in a hyperelastic material in a homogeneously simple-shear deformation state. For the plane-strain problem, homogeneous displacement can be defined by the deformation gradient $F_{11}=F_{22}=1$, $F_{12}=0$ and $F_{21}=\tan\gamma$, where γ denotes the shear angle of the simple-sheared deformation. Note that in this case the volume of the material is unchanged, i.e. $J=1$. Moreover, we consider the refraction of elastic waves normally incident on a simple-sheared hyperelastic material, as a schematic of the problem illustrated in Fig. 1. In this case, the plane interface is parallel to the shear direction. Therefore, the refraction angles of the P- and S-waves, which also denote the directions of ray velocities, can be yielded from the slowness curves at $\phi=0$.

To investigate the effect of two compressible versions of neo-Hookean models (W_{NH1} and W_{NH2}) on the elastic wave propagation, the slowness curves have been plotted in Fig. 2(a) and (b). For both SEFs, we choose $\lambda=4.32$ MPa, $\mu=1.08$ MPa, and $\rho=1050$ kg/m^3 as the initial material parameters, which refer to a compressible variant of material PSM-4 (Bertoldi and Boyce, 2008). The parameters are normalized to be $\lambda=4$, $\mu=1$ and $\rho=1$, for ease of the theoretical investigation. For the simple-shear deformation, the shear angle is set to be $\gamma=\arctan(1/3)$. It can be shown that the slowness curves of the S-waves turn out to have a similar shape. For P-waves, however, the slowness curves exhibit different orientations, leading to a significant difference in the directions of the ray velocities. As shown in Fig. 2(c), the ray direction of P-wave in material W_{NH1} is positive valued when the wave direction is in a range of $\phi\in[0,\ \pi/4]$. In contrast, the ray direction is negative for the case of W_{NH2}. Moreover, the polarization angles for the wave directions in a range of $\phi\in[0,\ \pi/4]$ have been plotted in Fig. 2(d), showing that elastic waves in material W_{NH1} are always in pure modes, which means the polarization directions are parallel (or normal) to the propagation directions of the P- (or S-) wave. Unlike W_{NH1}, only quasi elastic waves can be observed in W_{NH2}.

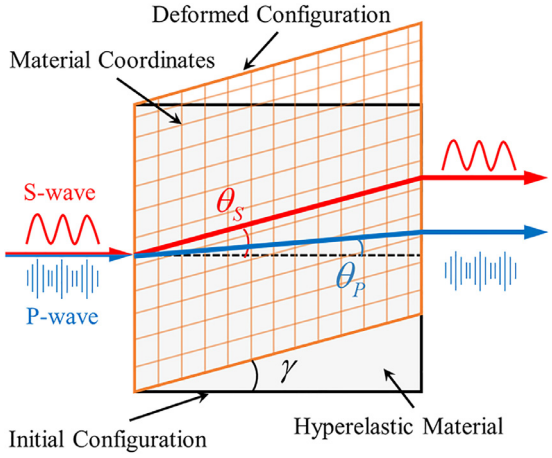

Fig. 1. Schematic diagram of elastic waves propagation and refraction in a hyperelastic material under simple-shear. The black and orange frames denote the initial and deformed configurations, respectively. The material coordinates are denoted by orange grids. γ is the shear angle. The blue and red lines represent the paths of P- and S-waves, respectively. θ_P and θ_S represent the refractive angles of P- and S-waves, respectively. In this case, the wave directions in the material is $\phi=0$.

To examine the influences of material parameters on elastic wave behavior in these hyperelastic models, slowness curves of the three hyperelastic materials W_{NH1}, W_{G1} and W_{AB1} with different material constants are provided in Fig. 3(a) and (b). The normalized initial parameters and the shear angle are also set to be $\lambda=4$, $\mu=1$, $\rho=1$ and $\gamma=\arctan(1/3)$. For W_{NH1}, $W_{G1}(J_m=10)$ and $W_{AB1}(N=1)$, considerable differences are noticeable in the slowness curves, as demonstrated in Fig. 3(a). However, for larger material constants, e.g. $J_m=20$ and $N=3$, the slowness curves almost coincide with each other. For the refraction problem described in Fig. 1, the influence of compressibility on the three models has been plotted in Fig. 3(c). Here, the normalized initial parameters and the shear angle are set to be $\mu=1$, $\rho=1$ and $\gamma=\arctan(1/3)$. λ/μ is introduced to represent the compressibility of the material. With the increase of the material incompressibility, the refraction angles of the P-waves significantly decrease, while that of the S-waves remain almost unchanged. Among the three models, W_{NH1} exhibits the largest separation angle. However, for $W_{AB1}(N=1)$, the corresponding separation angle is much smaller, and the two wave paths almost coincide when the material is nearly incompressible. Moreover, the influence of material constants on the refraction angles of the P- and S-waves has been plotted in Fig. 3(d). The normalized initial parameters and the shear angle are set to be $\lambda=4$, $\mu=1$,$\rho=1$ and $\gamma=\arctan(1/3)$. For larger material constants, the separation angles of the three SEFs tend to be consistent, because, in this case, both W_{G1} and W_{AB1} degenerate into W_{NH1}. However for smaller material constants, considerable differences in the separation angles are apparent for different SEFs.

Correspondingly, the influences of material constants and material compressibility on elastic wave behavior in materials W_{NH2} and W_{AB2} are demonstrated in Fig. 4. It is worth noting that the slowness curves of the P-waves in Fig. 4(a) and (b) have a different orientation with those shown in Fig. 3(a) and (b). This reveals that the ray directions of the P-waves are characterized by the two approaches used to construct the compressible SEFs. Considering the refraction problem, abnormal ray directions lead to negative refractions of P-waves for both SEFs derived from Approach II, which is

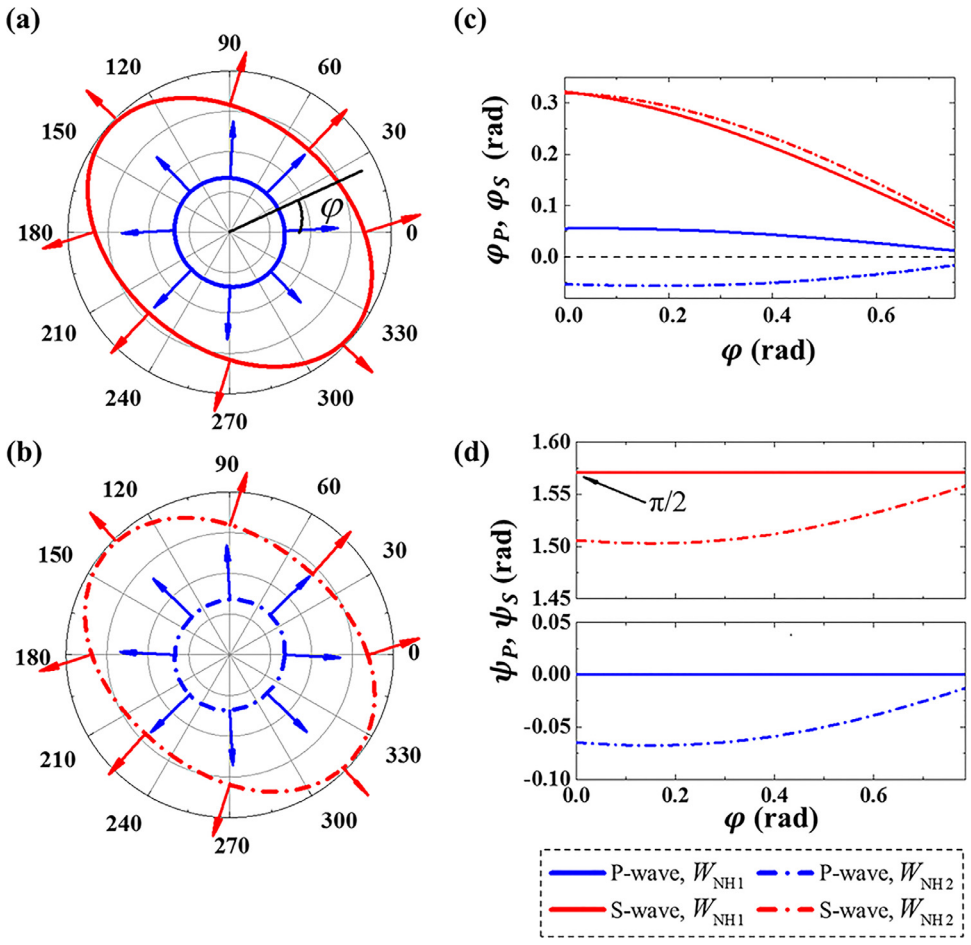

Fig. 2. Elastic waves propagation in simple-sheared neo-Hookean materials with the SEFs of W_{NH1} and W_{NH2}. (a) The slowness curves of the elastic waves propagating in the neo-Hookean material with SEF of W_{NH1}. ϕ denotes the wave direction. The arrows denote the directions of the ray velocities, (b) is the same as (a), but for the SEF of W_{NH2}, (c) the ray directions of the elastic waves with the wave direction of$\phi \in [0,\ \pi/4]$, (d) the polarization angles of the elastic waves with the wave direction of $\phi \in [0,\ \pi/4]$. For both SEFs, the normalized initial parameters are $\lambda = 4$, $\mu = 1$ and $\rho = 1$, the shear angle is $\gamma = \arctan(1/3)$.

distinct from that of the SEFs constructed by Approach I. This will consequently result in a larger separation angle of W_{AB2} than that of W_{NH2}, as shown in Fig. 4(c) and (d). It also should be noted that for all of the SEFs of Approach I, only W_{NH1} has the property of pure mode propagation.

To study the influence of the shear angle γ on the refraction properties of different SEFs, the separation angles are plotted with respect to the shear angle of the simple-shear deformation, as shown in Fig. 5. The normalized initial parameters for all the SEFs are $\lambda = 4$, $\mu = 1$ and $\rho = 1$. The material constants are set to be $J_m = 10$ for W_{G1}, and $N = 1$ for W_{AB1} and W_{AB2}. In the case of neo-Hookean materials (W_{NH1} and W_{NH2}), Fig. 5 clearly demonstrates the linear property of their capacity for bearing shear deformation, unlike those of the other models (W_{AB1}, W_{AB2} and W_{G1}). As the shear angle increases, the SEFs constructed by the different approaches exhibit diverse concavity. Two possible wave separation modes can be distinguished, which are bounded by the lines with respect to W_{NH1} and W_{NH2}. Evidently, this "mode separation" is due to the differences in the refraction properties of the P-waves.

5. Numerical validations

To validate the theoretical results in Section 4, numerical simulations have been performed by a two-step finite element model using the software COMSOL Multiphysics. In the first step, the finite deformation of the hyperelastic material is calculated using the solid mechanics module. Then, the deformed geometric configuration, together with the deformation gradient **F**, is imported into the second step in order to simulate the linear elastic wave motion governed by Eq. (9). In this step, the weak form PDE module is applied to deal with the asymmetry of the elastic tensor.

Consider a square hyperelastic material with the side length $l = 0.12$ m and the material parameters $\lambda = 4.32$MPa, $\mu = 1.08$MPa and $\rho = 1050$ kg/m^3. By applying the displacement field $U_y = (x + 0.6)/30$ m to the model, a homogeneous simple-sheared deformation can be obtained with the shear angle γ satisfying $\tan\gamma = 1/3$. As illustrated in Fig. 1, on the left side of the square, a P-wave beam and an S-wave beam are normally input at the same position. Both the incident waves are set with the maximum amplitude as $u = 1 \times 10^{-3}$ m, and with the angular frequencies of the S-wave and the P-wave being $\omega_S = 0.3$ MHz and $\omega_P = 12.9$ MHz, respectively.

In general, the results of the numerical simulations are in excellent agreement with those obtained from theoretical analyses. The total displacement fields of the P- and S-waves propagated in material W_{NH1} and W_{NH2} are illustrated in Fig. 6(a) and (b), respectively. Comparing these two figures, it is clearly evident that the S-waves have similar refraction angles, whereas the P-waves exhibit the opposite behavior. To better observe quasi wave modes in material W_{NH2}, the x- and y-components of the displacement field are illustrated in Fig. 6(c) and (d), respectively. The small x- (or y-) displacement on the S- (or P-) wave path (shown in the insets in Fig. 6(c) and (d)) clearly demonstrates the polarization of the wave

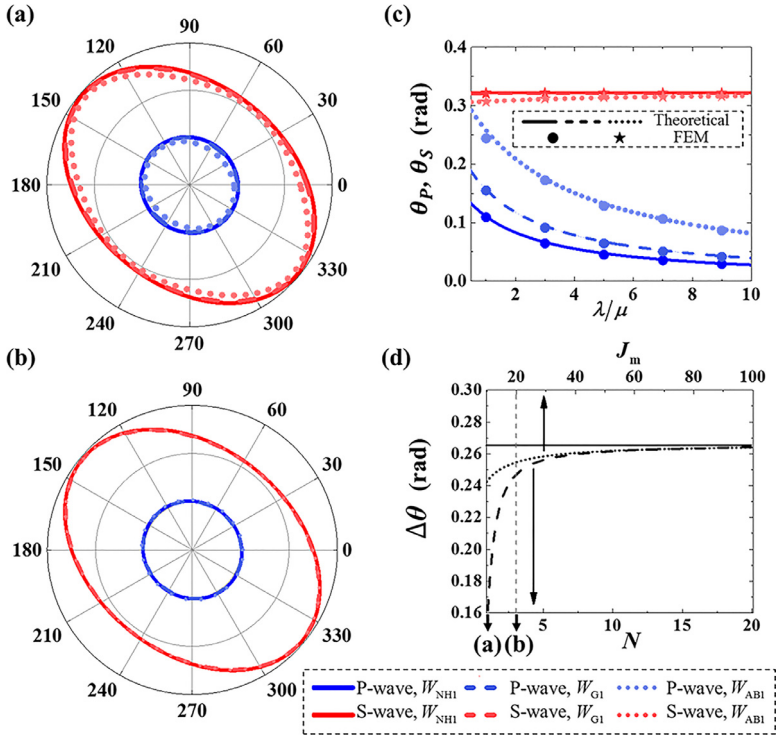

Fig. 3. Elastic waves propagation and refraction in simple-sheared hyperelastic materials with the SEFs of W_{NH1}, W_{G1} and W_{AB1}. (a) The slowness curves of the elastic waves propagating in the hyperelastic materials with the SEFs of W_{NH1}, $W_{G1}(J_m = 10)$ and $W_{AB1}(N = 1)$, (b) is the same as (a), but for W_{NH1}, $W_{G1}(J_m = 20)$ and $W_{AB1}(N = 3)$. In both (a) and (b), the normalized initial parameters are $\lambda = 4$, $\mu = 1$ and $\rho = 1$, the shear angle is $\gamma = \arctan(1/3)$, (c) the refraction angles of the elastic waves with different material compressibility $\lambda/\mu \in (0.5,\ 10]$ for W_{NH1}, $W_{G1}(J_m = 10)$ and $W_{AB1}(N = 1)$, respectively. The initial mass density is $\rho = 1$, the shear angle is $\gamma = \arctan(1/3)$ and the wave direction is $\phi = 0$, (d) the angle between refracted P- and S-waves with different material constants J_m and N. The normalized initial parameters are $\lambda = 4$, $\mu = 1$ and $\rho = 1$, the shear angle is $\gamma = \arctan(1/3)$, and the wave direction is $\phi = 0$.

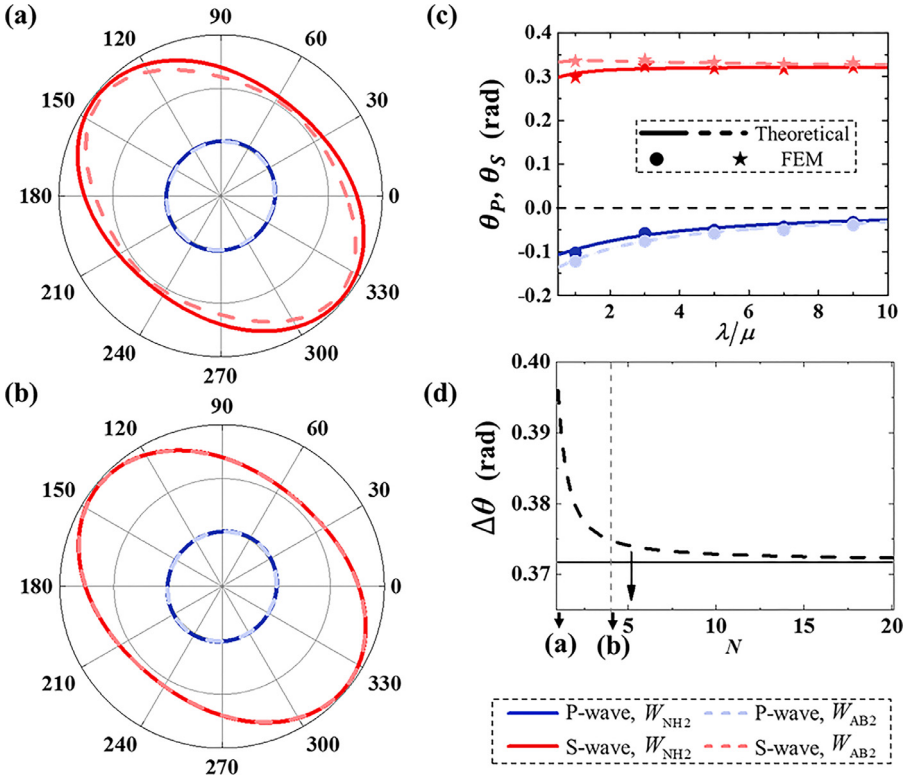

Fig. 4. Elastic waves propagation and refraction in simple-sheared hyperelastic materials with the SEFs of W_{NH2} and W_{AB2}. (a) The slowness curves of the elastic waves propagating in the hyperelastic materials with the SEFs of W_{NH2} and $W_{AB2}(N = 1)$, (b) is the same as (a), but for W_{NH2} and $W_{AB2}(N = 3)$. In both (a) and (b), the normalized initial parameters are $\lambda = 4$, $\mu = 1$ and $\rho = 1$, the shear angle is $\gamma = \arctan(1/3)$, (c) the refraction angles of the elastic waves with different material compressibility $\lambda/\mu \in (0.5,\ 10]$ for W_{NH2} and $W_{AB2}(N = 1)$. The initial mass density is $\rho = 1$, the shear angle is $\gamma = \arctan(1/3)$ and the incident angle is $\phi = 0$, (d) the angle between refracted P- and S-waves with different material constant N. The normalized initial parameters are $\lambda = 4$, $\mu = 1$ and $\rho = 1$, the shear angle is $\gamma = \arctan(1/3)$, and the incident angle is $\phi = 0$.

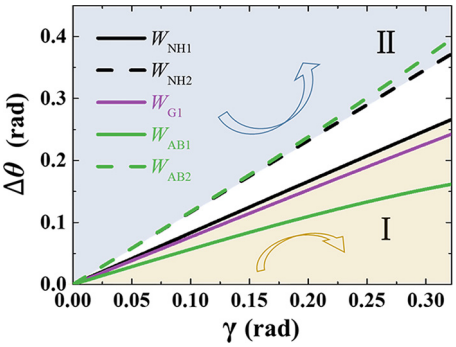

Fig. 5. The wave separation angle between refracted P- and S-waves with respect to different shear angle γ. The shaded areas I and II represent two possible wave separation modes. The normalized initial parameters are $\lambda = 4$, $\mu = 1$ and $\rho = 1$, the shear angle is $\gamma = \arctan(1/3)$, and the wave direction is $\phi = 0$. $J_m = 10$ for W_{G1}, and $N = 1$ for W_{AB1} and W_{AB2}.

propagation. As expected, no similar result can be observed in material W_{NH1}.

The distributions of the displacements on the right boundary of the materials (the green line in Fig. 6(a) and (b)), are illustrated in Fig. 7. Both the P- and S-wave fields, as shown in Fig. 7(a) and (b), are distributed on the right side of the auxiliary line denoting the position of the incident wave. On the contrary, in Fig. 7(c) and (d), the P- and S-wave fields are distributed in different sides, indicating the property of negative refraction. With the verification of some other SEFs, i.e. the exponentiated Hencky-logarithmic energy (Lankeit et al., 2015) as discussed in the Supplementary Material, we therefore hypothesize that such negative refraction is a common feature for the SEFs constructed by Approach II. Moreover, in Fig. 7(a), W_{AB1} and W_{G1} demonstrate minor perturbations of the wave fields for small material constants. The perturbations reduce to the same level as that of W_{NH1} for larger material constants, as shown in Fig. 7(b). These findings recall the results in Section 4 where the pure mode propagation property is unique for W_{NH1}, and once again confirmed the similar refraction behavior among W_{NH1}, W_{AB1} and W_{G1} with large material constants. For the SEFs constructed by Approach II, however, the perturbations are always present regardless of any SEF and material constants, as shown in Fig. 7(c) and (d).

6. Discussion and conclusion

In this work, we have investigated the propagation and refraction of elastic waves in pre-deformed hyperelastic materials with different SEFs. By conducting both theoretical and numerical analyses, significantly different results can be found for the models constructed by the two SEF extension approaches. The variety of qualitatively different wave propagation behaviors gives us the opportunity to design novel architected materials with exotic functionalities.

In particular, we have discovered that W_{NH1} exhibits pure mode propagation of elastic waves when the material is subjected to pre-deformation. Such a behavior is anomalous for hyperelastic materials and therefore, can be beneficial for the manipulation of elastic waves on the basis of Hyperelastic Transformation theory (Parnell, 2012; Parnell et al., 2012; Chang et al., 2015). It is also worth noting that W_{AB1} and W_{G1} with relatively large material constants have similar wave behaviors as that of W_{NH1}, and can also manipulate S-waves, albeit not as accurately as W_{NH1}.

On the separation of P- and S-waves, the SEFs constructed by Approach I and II have their own merits. The elimination of dealing with polarization makes W_{NH1} more efficient at transmitting and receiving elastic waves without energy loss. On the other hand, SEFs constructed by Approach II have the advantage of large separation angles, which can be crucially important for some small-scale applications. The effects of material compressibility, material constant and shear angle on the separation angle were also investigated. The results demonstrated that for the SEFs constructed by Approach I, the higher the material incompressibility is, the larger the separation angle is, which is contrary to the SEFs constructed by Approach II. Moreover, for all the SEFs, larger wave separation angles can be achieved using either smaller material constants or larger shear angles.

This work also promotes an interesting and challenging direction for material fabrication. With the development of modern chemical synthesis processes (Chen et al., 2017), more elaborate theory and methodology are needed to precisely fabricate a

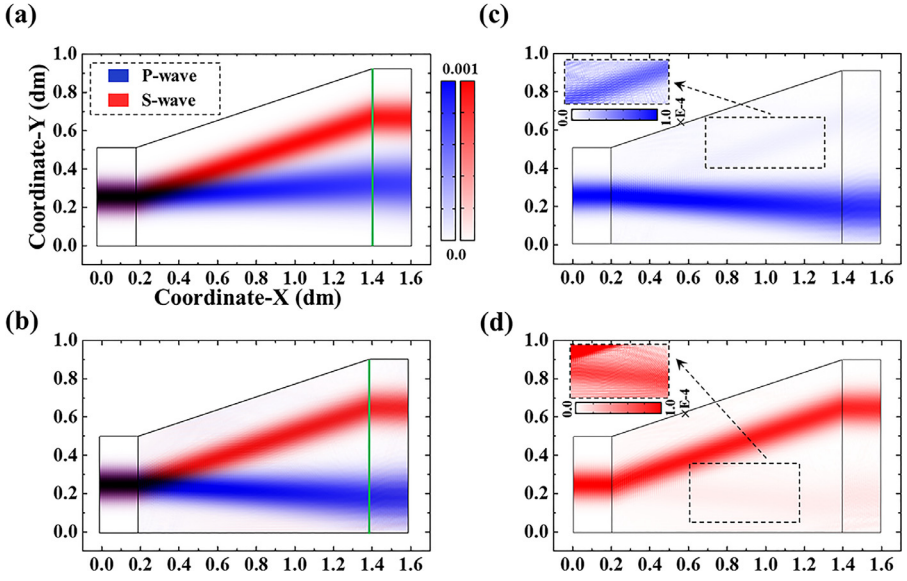

Fig. 6. Displacement fields in hyperelastic materials under simple shear. (a) Total displacement field in simple-sheared neo-Hookean material with the SEF of W_{NH1}, (b) the same as (a), but for W_{NH2}. Fig. (c) and (d) are the corresponding displacement components u_x and u_y with Fig. (b). (a) (For interpretation of the references to color in this figure legend, the reader is referred to the web version of this article.).

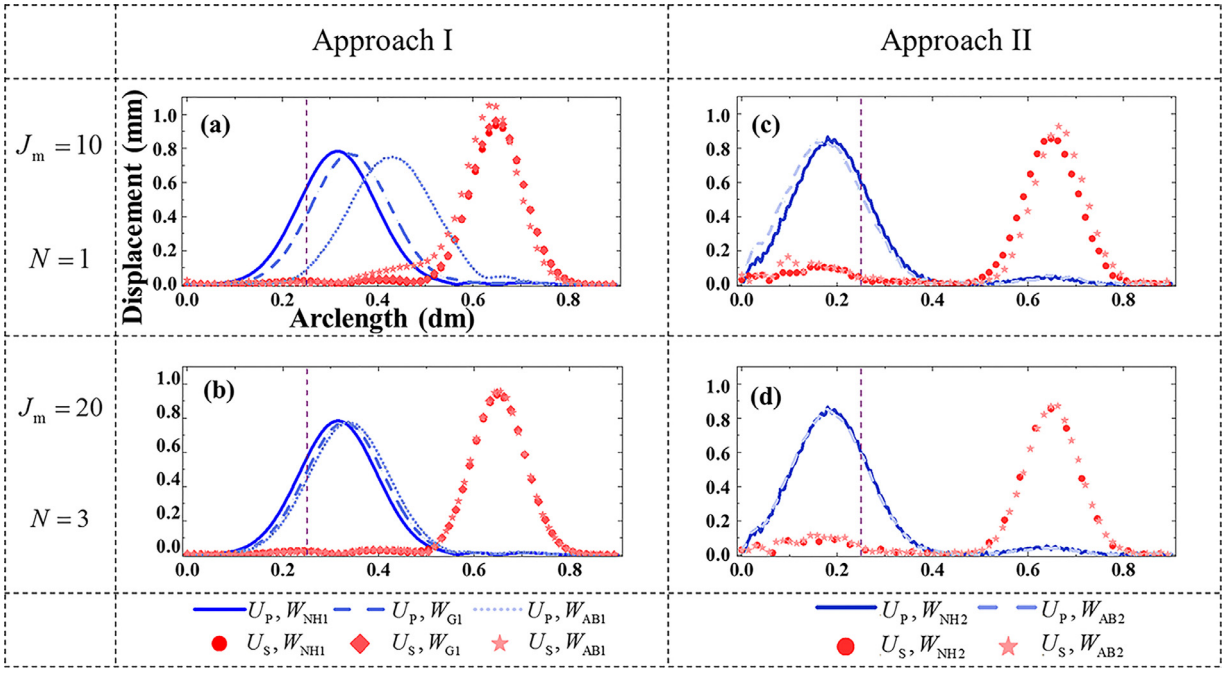

Fig. 7. Total displacement on auxiliary segments (green lines in Fig. 6) for the different cases. The purple lines denote the position of the horizontal incident waves. (a) (For interpretation of the references to color in this figure legend, the reader is referred to the web version of this article.).

material based on the criteria of a particular SEF. Only in this way can we freely take advantage of the distinguishing features among different SEFs.

Acknowledgment

The authors would like to thank Prof. Rui Zhu and Mr. Andres Faraone-Pirie for their assistance in proofreading. This work was supported by the National Natural Science Foundation of China (Grant No. 11602294) and the Fundamental Research Funds for the Central Universities (Grant Nos. 2017QC056 and 2017LX002).

Supplementary materials

Supplementary material associated with this article can be found, in the online version, at doi:10.1016/j.ijsolstr.2017.07.027.

References

Arruda, E.M., Boyce, M.C., 1993. A three-dimensional constitutive model for the large stretch behavior of rubber elastic materials. J. Mech. Phys. Solids. 41, 389–412.
Auld, B.A., 1973. Acoustic Fields and Waves in Solids. Wiley.
Auriault, J.L., Boutin, C., 2012. Long wavelength inner-resonance cut-off frequencies in elastic composite materials. Int. J. Solids. Struct. 49, 3269–3281.
Bertoldi, K., Boyce, M.C., 2008. Wave propagation and instabilities in monolithic and periodically structured elastomeric materials undergoing large deformations. Phys. Rev. B 78, 2599–2604.
Bischoff, J.E., Arruda, E.M., Grosh, K., 2001. A new constitutive model for the compressibility of elastomers at finite deformations. Rubber Chem. Technol. 74, 541–559.
Boyce, M.C., Arruda, E.M., 2012. Constitutive models of rubber elasticity: a review. Rubber Chem. Technol. 73, 504–523.
Chang, Z., Guo, H.-Y., Li, B., Feng, X.-Q., 2015. Disentangling longitudinal and shear elastic waves by neo-Hookean soft devices. Appl. Phys. Lett. 106, 16.
Chen, Q., Yu, X., Pei, Z., Yang, Y., Wei, Y., Ji, Y., 2017. Multi-stimuli responsive and multi-functional oligoaniline-modified vitrimers. Chem. Sci. 8, 724–733.
Ehlers, W., Eipper, G., 1998. The simple tension problem at large volumetric strains computed from finite hyperelastic material laws. Acta Mech. 130, 17–27.
Gent, A., 1996. A new constitutive relation for rubber. Rubber Chem. Technol. 69, 59–61.
Hartmann, S., Neff, P., 2003. Polyconvexity of generalized polynomial-type hyperelastic strain energy functions for near-incompressibility. Int. J. Solids. Struct. 40, 2767–2791.
Kaliske, M., Rothert, H., 1997. On the finite element implementation of rubber-like materials at finite strains. Eng. Comput. 14, 216–232.
Lankeit, N.P., Ghiba, ID., Martin, R., Steigmann, D., 2015. The exponentiated Hencky-logarithmic strain energy. Part II: Coercivity, planar polyconvexity and existence of minimizers. Z. Angew. Math. Phys. 66, 1671.
Liu, Y., Chang, Z., Feng, X.Q., 2016. Stable elastic wave band-gaps of phononic crystals with hyperelastic transformation materials. Extreme Mech. Lett. 11, 37–41.
Norris, A.N., Parnell, W.J., 2012. Hyperelastic cloaking theory: transformation elasticity with pre-stressed solids. P. Roy. Soc. A 468, 2881–2903.
Ogden, R.W., 1972. Large deformation isotropic elasticity - on the correlation of theory and experiment for incompressible rubberlike solids. P. Roy. Soc. Lond. A 326, 565–584.
Ogden, R.W., 1997. Non-linear Elastic Deformations. Courier Corporation.
Ogden, R.W., 2007. Incremental statics and dynamics of pre-stressed elastic materials. CISM Courses Lect. 495, 1–26.
Parnell, W.J., 2012. Nonlinear pre-stress for cloaking from antiplane elastic waves. Proc. R. Soc. A 468, 563–580.
Parnell, W.J., Norris, A.N., Shearer, T., 2012. Employing pre-stress to generate finite cloaks for antiplane elastic waves. Appl. Phys. Lett. 100, 171907.
Rokhlin, S.I., Bolland, T.K., Adler, L., 1985. Reflection and refraction of elastic waves on a plane interface between two generally anisotropic media. J. Acoust. Soc. Am. 77, 447–449.
Shim, J., Wang, P., Bertoldi, K., 2015. Harnessing instability-induced pattern transformation to design tunable phononic crystals. Int. J. Solids. Struct. 58, 52–61.
Simo, J.C., Pister, K.S., 1984. Remarks on rate constitutive equations for finite deformation problems: computational implications. Comput. Method. Appl. M 46, 201–215.
Wang, L., Bertoldi, K., 2012. Mechanically tunable phononic band gaps in three-dimensional periodic elastomeric structures. Int. J. Solids. Struct. 49, 2881–2885.
Yeoh, O., 1993. Some forms of the strain energy function for rubber. Rubber Chem. Technol. 66, 754–771.